AGU PUBLICATIONS

JGR

Journal of Geophysical Research: Oceans

RESEARCH ARTICLE

10.1002/2017JC013542

Key Points:
- Most of the nitrate (>90%) used by phytoplankton to grow in the Great Australian Bight has been recycled locally
- Phytoplankton growth within the Great Australian Bight peaks in spring and autumn and has a subsurface maximum
- Weak stratification and topographical uplift facilitate phytoplankton growth in the Great Australian Bight

Supporting Information:
- Figure S1

Correspondence to:
P. Cetina-Heredia,
p.cetinaheredia@unsw.edu.au

Citation:
Cetina-Heredia, P., van Sebille, E., Matear, R. J., & Roughan, M. (2018). Nitrate sources, supply, and phytoplankton growth in the Great Australian Bight: An Eulerian-Lagrangian modeling approach. *Journal of Geophysical Research: Oceans*, *123*, 759–772. https://doi.org/10.1002/2017JC013542

Received 12 NOV 2017
Accepted 20 DEC 2017
Accepted article online 28 DEC 2017
Published online 1 FEB 2018

Nitrate Sources, Supply, and Phytoplankton Growth in the Great Australian Bight: An Eulerian-Lagrangian Modeling Approach

Paulina Cetina-Heredia[1], Erik van Sebille[1,2,3], Richard J. Matear[4], and Moninya Roughan[5]

[1]Climate Change Research Centre, ARC Centre of Excellence for Climate System Science, UNSW Australia, Sydney, Australia, [2]Department of Physics, Grantham Institute, Imperial College London, London, UK, [3]Institute for Marine and Atmospheric Research, Utrecht University, Utrecht, Netherlands, [4]CSIRO Marine Laboratories, CSIRO Marine and Atmospheric Research, Hobart, Australia, [5]Regional and Coastal Oceanography Laboratory, School of Mathematics and Statistics, UNSW Australia, Sydney, Australia

Abstract The Great Australian Bight (GAB), a coastal sea bordered by the Pacific, Southern, and Indian Oceans, sustains one of the largest fisheries in Australia but the geographical origin of nutrients that maintain its productivity is not fully known. We use 12 years of modeled data from a coupled hydrodynamic and biogeochemical model and an Eulerian-Lagrangian approach to quantify nitrate supply to the GAB and the region between the GAB and the Subantarctic Australian Front (GAB-SAFn), identify phytoplankton growth within the GAB, and ascertain the source of nitrate that fuels it. We find that nitrate concentrations have a decorrelation timescale of ~60 days; since most of the water from surrounding oceans takes longer than 60 days to reach the GAB, 23% and 75% of nitrate used by phytoplankton to grow are sourced within the GAB and from the GAB-SAFn, respectively. Thus, most of the nitrate is recycled locally. Although nitrate concentrations and fluxes into the GAB are greater below 100 m than above, 79% of the nitrate fueling phytoplankton growth is sourced from above 100 m. Our findings suggest that topographical uplift and stratification erosion are key mechanisms delivering nutrients from below the nutricline into the euphotic zone and triggering large phytoplankton growth. We find annual and semiannual periodicities in phytoplankton growth, peaking in the austral spring and autumn when the mixed layer deepens leading to a subsurface maximum of phytoplankton growth. This study highlights the importance of examining phytoplankton growth at depth and the utility of Lagrangian approaches.

1. Introduction

The Great Australian Bight (GAB) is a coastal sea along southern Australia with unique biodiversity providing important habitat for endemic and endangered species such as the Australian sea lion and the southern right whale (Gill et al., 2011; Petrusevics et al., 2009). Importantly, the GAB sustains the largest finfish fishery in the region (McClatchie et al., 2006) acting as spawning grounds for anchovies (*Engraulis australis*, Dimmlich et al., 2004) and sardines (*Sardinops sagax*), and feeding grounds for larger pelagic fish (Ward et al., 2006). Phytoplankton growth is the foundation for energy transfer into higher trophic levels (Falkowski & Kolber, 1995); however, the sources of nutrients consumed by phytoplankton during growth remain unknown, and the spatiotemporal patterns of phytoplankton growth sustaining the ecosystem in the GAB have received little attention.

Wind-driven upwelling events have been identified on the eastern side of the GAB and linked to the supply of deep water with nutrient concentrations considerably larger than those in the background (Lewis, 1981). Moreover, Kämpf et al. (2004) showed surface chlorophyll-a concentrations peak following these upwelling events. While locally important, such events are limited in time and space; specifically, they are constrained to summer periods and occur in the Eyre Peninsula, Kangaroo Island, and Bonney Coast covering approximately a third of the GAB shelf. Therefore, wind-driven upwelling events have little impact on the seasonal cycle of chlorophyll in the region as a whole (Condie & Dunn, 2006), contributing to productivity locally. Recently, Kämpf and Kavi (2017) examined monthly images of satellite-derived chlorophyll-a concentrations and found evidence of moderate widespread autumn phytoplankton blooms, which extend across the whole width of the GAB and have the potential to sustain the top predator biomass in the GAB.

Although phytoplankton blooms within the GAB have been examined before (e.g., Kämpf et al., 2004, van Ruth, 2009), most of the studies are either local in scope, use in situ measurements over short time periods, or are based on satellite-derived chlorophyll-a concentrations. Satellite ocean color images and measurements of sea surface temperature and fluorescence are useful tools to examine phytoplankton blooms and estimate primary productivity (e.g., Behrenfeld & Falkowski, 1997, Xing et al., 2007). However, satellites are unable to observe properties at depth (Lavigne et al., 2012) and subsurface chlorophyll-a maxima are common in the Australasian region where they can represent a large fraction of the total phytoplankton biomass in the water column (Condie & Dunn, 2006). Within the GAB, van Ruth (2009) found the highest chlorophyll-a concentrations at ~35 m in the eastern GAB, and estimated more than 50% of total productivity occurred below the surface mixed layer. Here we use outputs of a coupled hydrodynamic-biogeochemical model that allows examining phytoplankton growth within the GAB for the entire euphotic zone over a 12 year time period (1992–2005).

Phytoplankton growth is regulated by multiple factors including light, temperature, and nutrient availability (Boyd et al., 2010). Nitrate and iron are the most common nutrients limiting phytoplankton growth globally (Moore et al., 2013). Iron supply from sediments is greatest over the continental shelves (Wadley et al., 2014); thus, iron concentrations are typically higher closer to the coast (Graham et al., 2015), and iron is not expected to limit phytoplankton growth in the GAB (http://www.ga.gov.au/corporate_data/70156/70156.pdf). In contrast, the observational synthesis by Condie and Dunn (2006) showed that north of the Subtropical Australian Front (SAFn), where the GAB lies, nitrate is likely to be a limiting nutrient. The high nitrate concentrations occur deep in the open ocean such as Southern Ocean waters and this study examines the sources of nitrate to the GAB euphotic layer.

The GAB receives water from adjacent oceans (i.e., Pacific, Indian, and Southern). Hydrographic samples have revealed that the Flinders Current, flowing westward across the GAB, carries Subantarctic Mode Water from the Southern Ocean (Richardson et al., 2009), and that the Leeuwin Current, flowing eastward across the GAB, brings Subtropical Surface Water from the Indian Ocean (Richardson et al., 2009; Yit Sen Bull & van Sebille, 2016). These water masses have different nitrate concentrations and it is unclear which water masses provides the nitrate that is used for phytoplankton growth in the GAB, the mechanism that makes it available for phytoplankton uptake, and how the supply changes over time.

Here we use an Eulerian-Lagrangian approach to identify phytoplankton growth within the GAB and relate it to nitrate sources and supply. We characterize phytoplankton growth events in space and time over a 12 year period, and use this analysis to provide insight into mechanisms facilitating the nitrate supply to fuel phytoplankton growth.

2. Method

2.1. Model

Outputs of a coupled hydrodynamic-biogeochemical ocean model are used to track water parcels going into the GAB and examine changes of nitrate and phytoplankton concentrations along their trajectories. The Whole Ocean Model of Biogeochemistry And Trophic-dynamics (WOMBAT; Kidston et al., 2011; Matear et al., 2013) is a Nutrient, Phytoplankton, Zooplankton, and Detritus (NPZD) model that has been incorporated into the hydrodynamic, eddy-resolving, Ocean Forecast Australian Model (OFAM; Oke et al., 2013). OFAM has a spatial resolution of 1/10° that yields an adequate modeling of currents around Australia (Sun et al., 2012). Matear et al. (2013) showed that modeled spatial patterns and seasonal evolution of phytoplankton in the Tasman Sea and Southern Ocean agree with satellite observations. OFAM-WOMBAT outputs have been used to study sources of iron in the western Pacific (Qin et al., 2016); furthermore, recent studies have implemented the WOMBAT model to look at phytoplankton dynamics in East Australia (Laiolo et al., 2016), and the phytoplankton response to future climate change (Matear et al., 2015; Zhang et al., 2016).

Comparisons of horizontal and vertical distributions of modeled nitrate concentrations with observations compiled into the CSIRO Atlas of Regional Seas (CARS, released in 2009; Ridgway & Dunn, 2003) show that the observed spatial distribution of low nitrate concentrations close to the coast and high nitrate concentrations in the Southern Ocean is replicated in the model (Figures 1a and 1b). However, the model depicts more spatial variability than the CARS observations. This may in part reflect the limited observational coverage and the coarse resolution of CARS (1°), which makes CARS overly smooth. The model captures well the

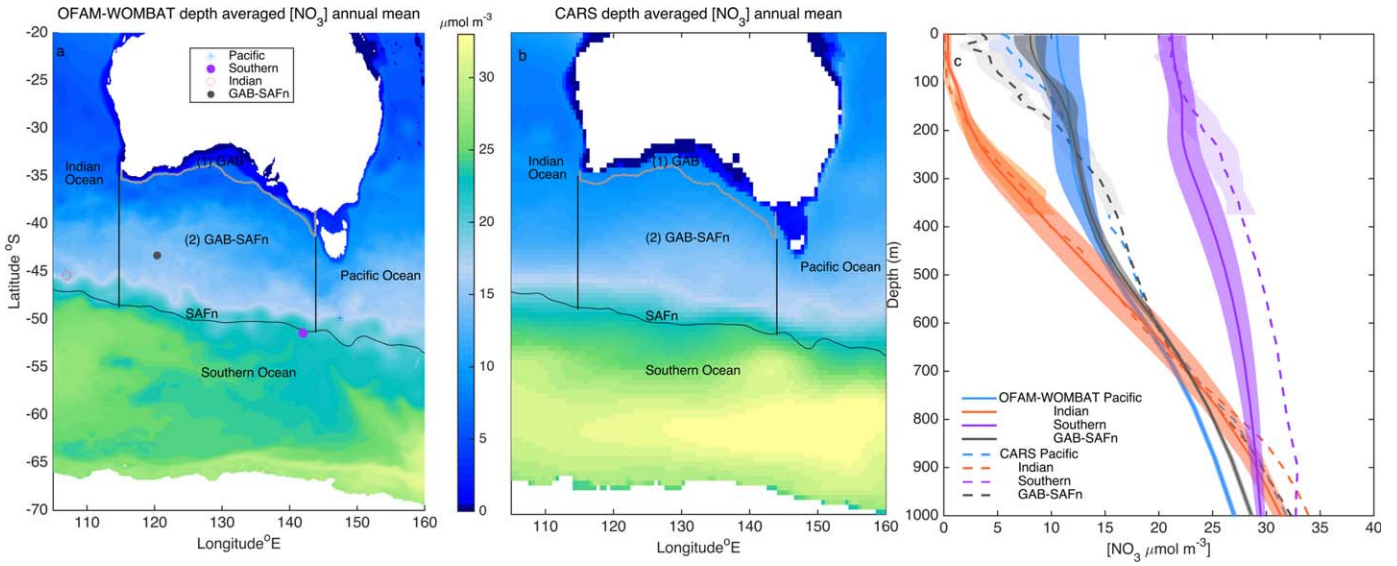

Figure 1. (a) Depth-averaged (surface 1,000 m) annual mean of NO_3 concentration from OFAM-WOMBAT (1996) and (b) CARS. (c) Vertical profiles of the annual mean and standard deviation of nitrate concentrations at locations within each source (i.e., Pacific, Southern, Indian Oceans, and GAB-SAFn, shown by symbols in plot a). Solid lines are model outputs and dashed lines are CARS observations. In plot (a), the grey line shows the GAB limit (2,000 m isobath), and the black lines show the boundaries between different regions (i.e., Pacific, Southern, Indian Oceans, and GAB-SAFn) and the horizontal boundaries of boxes (1 GAB and 2 GAB-SAFn) through which nitrate fluxes are calculated.

order of magnitude, variability, and change over depth of annual mean nitrate concentrations at specific locations in the Pacific, Southern, Indian oceans, and the region between the GAB and the SAFn (Figure 1c).

Similarly, we compare daily surface chlorophyll-a concentrations from OFAM-WOMBAT with those from satellite observations from 1997 to 2005. The satellite observations (GlobColour data, http://globcolour.info) used in this study are developed, validated, and distributed by ACRI-ST, France. Modeled phytoplankton concentrations are transformed to chlorophyll-a concentrations considering a 50:1 mg C:chl-a ratio, and a 16:106 mol N:C Redfield ratio; yielding 1 mmol of N equivalent to 1.59 mg of chlorophyll-a (Matear et al., 2013). Spatial maps of mean chlorophyll-a show the model captures the distribution of regions of high and low chlorophyll-a concentrations (supporting information Figure S1); spatial maps of the root mean squared difference (RMSD) between the observed and modeled fields are used to assess the model's performance capturing temporal variability of chlorophyll fields; the maps show that deviations of the model from observations are often 3–4 times smaller than typical standard deviation values of observed chlorophyll-a concentrations within the GAB. Generally, there is better agreement where more observations are available for comparison (Figure 2). Overall, OFAM-WOMBAT provides a reasonable representation of phytoplankton and motivates us to use it to examine phytoplankton growth within the GAB and link to relate the phytoplankton growth to nitrate sources using an Eulerian-Lagrangian approach.

2.2. Eulerian-Lagrangian Approach

Using combined Eulerian-Lagrangian approaches to investigate ocean biogeochemistry has a number of advantages (Chenillat et al., 2015). For instance, an increase in phytoplankton concentrations along a water parcel trajectory (Lagrangian) corresponds to phytoplankton growth, whereas an increase in phytoplankton concentration at a fixed location can also be due to advection of biomass into the fixed observational frame (Jönsson et al., 2011; Jönsson & Salisbury, 2016). Thus, using a Lagrangian approach is attractive to diagnosing phytoplankton growth. In addition, the interplay between physical and chemical forcings and the phytoplankton response can be monitored (D'Ortenzio et al., 2014); in this study, we focus on water parcel trajectories preceding phytoplankton growth to reveal nitrate sources and mechanisms facilitating nitrate delivery into regions where phytoplankton consumes it. Finally, the use of model outputs and water parcel trajectories in three dimensions gives spatial and depth information on the nitrate sources for phytoplankton growth.

Here we use backward and forward water parcel trajectories to, respectively, reveal: (1) where the nitrate consumed by phytoplankton growth comes from and (2) where and when the phytoplankton inside the

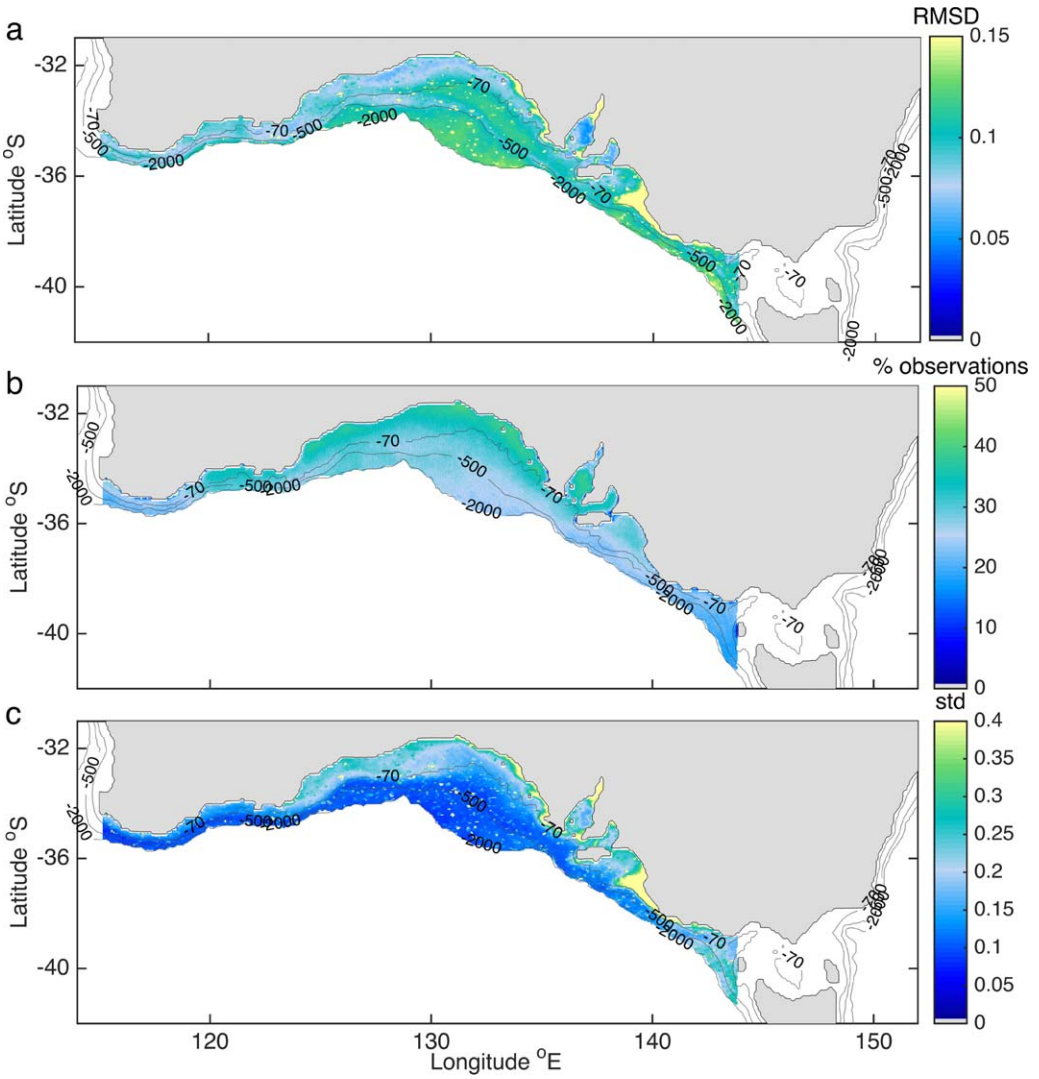

Figure 2. (a) Map of the root mean squared difference (RMSD) between satellite and modeled daily surface chlorophyll-a concentration. Data have been analyzed in bins of 4 × 4 km (satellite spatial resolution) and processed for the period of January 1997 to December 2005. (b) Percentage of observations for each bin relative to the number of days over the period of January 1997 to December 2005. (c) Map of the standard deviation of satellite chlorophyll-a concentration over the period of January 1997 to December 2005.

GAB grow. Water parcel trajectories are simulated offline with the Connectivity Modeling System (CMS; Paris et al., 2013), a Lagrangian tracking algorithm, using three-dimensional daily velocities simulated by OFAM-WOMBAT. Neutrally buoyant "particles" are seeded daily from June 1993 to June 2005, throughout the water column, along the 2,000 m isobath delimiting the GAB (Figure 1), in grid cells spaced every 1/10° horizontally, every 10 m vertically in the top 200 m and between 11 and 173 m as it gets deeper to 2,000 m. Particles are only released at times and locations when the instantaneous flow advects water parcels into the GAB; thus, the positions and spacing between seeded particles varies daily. This results in a total of approximately 2.5×10^6 particle trajectories, with an average of ~600 particles released per day. The position (longitude, latitude, and depth) of the water parcels is recorded daily and OFAM-WOMBAT nitrate and phytoplankton concentrations are interpolated onto the water parcel trajectories for further analysis.

Particles are advected backward in time with OFAM three-dimensional daily velocity fields without additional horizontal or vertical diffusion. Both the horizontal and vertical diffusions are parameterized in the hydrodynamic model; good agreement between observed and modeled nitrate horizontal distributions and vertical profiles (Figure 1) implies that horizontal and vertical diffusion processes are resolved well by

the hydrodynamic model, respectively, and particle advection suffices to capture tracers distribution. Moreover, larger changes in nutrient concentration are more likely a consequence of biological activity than vertical diffusion. For instance, Qin et al. (2015) show that in the Pacific Ocean, changes in iron concentration due to vertical diffusion are an order of magnitude smaller than those caused by scavenging. Thus, neglecting further effects of vertical diffusion on nitrate concentrations distributions is reasonable. Similarly, in the oligotrophic water of the region, if a parcel of water gets into the mixed layer depth (MLD) its nutrients will be almost completely used by biological processes and reduced to nearly zero. Thus, its vertical diffusion within the MLD (where diffusion is expected to be largest in magnitude) would not have the time to affect nutrient distributions before they are used.

2.3. Nitrate Local Sources

The distribution of nitrate in the ocean is determined by physical (i.e., advection and diffusion), and biological processes (Williams & Follows, 2003). Assuming diffusion is small, changes of nitrate concentration along water parcel trajectories are the result of biological activity (i.e., phytoplankton uptake and organic matter remineralization). Thus, nitrate concentration is not expected to decrease considerably unless it is utilized for phytoplankton growth.

In Lagrangian simulations, one question is always for how much time to track the particles. In principle, the particles could be tracked back for years. However, it is unlikely that nitrate concentrations years before a particle reached the GAB are relevant for what happens there. In order to set a time limit on what can be called the origin of nitrate, we need an estimate of how fast nitrate varies along the particle trajectories. We particularly focus on departures from the nitrate concentration at the moment nitrate is taken up by phytoplankton. Here we use the decorrelation time scale of nitrate anomalies to provide an estimate of this time scale, which we will henceforth call the nitrate memory time. The idea is that the moment that the nitrate concentration anomaly is not autocorrelated anymore is a proxy of the origin of nitrate of a water parcel. Once we quantify this nitrate memory time, we identify the location of the water parcel at that time; we separate the source regions (Figure 1) into the Pacific, Southern, Indian Ocean, the GAB, or the region between the GAB and Subantarctic Australian Front (GAB-SAFn). We define the GAB as the region between the coast and the 2,000 m isobath. We use Sallée et al. (2008) sea surface height and temperature gradients criteria to define the Subantarctic Australian Front. A record of the date, location, and intensity of each phytoplankton growth instance is kept to examine how they relate to the various nitrate source regions.

The nitrate memory time is calculated individually for each water parcel trajectory associated with a phytoplankton growth instance. The nitrate concentrations along the backward trajectory of each water parcel are used to construct time series prior to phytoplankton growth. The autocorrelation of the time series indicates the statistical dependence of the variable over time; and the decorrelation time scale (time-lag of the first zero crossing) indicates significant changes in the variable (Talley et al., 2011). We therefore compute autocorrelations of time series of nitrate concentration anomalies and use the decorrelation time scale to determine the nitrate memory time (Figure 3). The time series of nitrate concentration anomalies are constructed by subtracting the mean nitrate concentration from all the time series values. The decorrelation time or nitrate memory time allows us to set a limit on the time we follow a water parcel where phytoplankton grows, backward in time, before determining the source of the nitrate taken up by phytoplankton.

2.4. Nitrate Supply

Even if there is local recycling of nitrate along the path of water parcels, nitrate can be originally supplied or advected from afar. Thus, besides identifying local nitrate sources, we calculate the exchange of nitrate across the boundaries of two boxes, one that encompasses the GAB, from the coastline up to the 2,000 m isobath, and a second covering a region between the GAB and the Sub Antarctic Front (i.e., GAB-SAFn, Figure 1). The daily across boundary and depth integrated nitrate flux through each box over 12 years (1992–2005) is calculated as:

$$NF = \int_{z=H(x)}^{z=0} \int [v(x,z)N(x,z)]dx\ dz$$

where dx is the horizontal dimension along the boundary of the box, dz is the vertical dimension between the surface and the bottom depth H, v is the velocity perpendicular to the box, and N is the nitrate concentration on the face of the box.

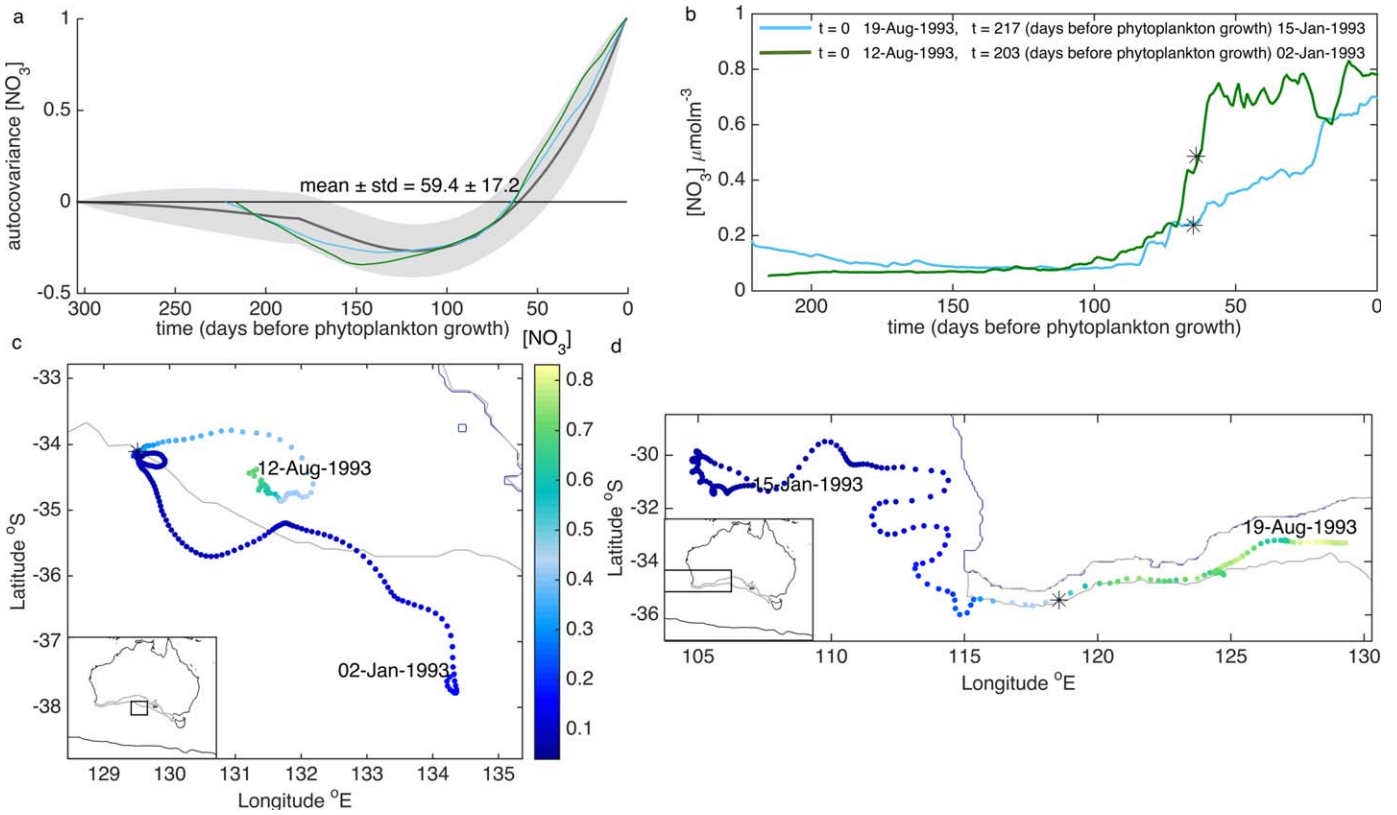

Figure 3. (a) Autocorrelation of nitrate concentration anomalies along backward water parcel trajectories. The mean (black line) and standard deviation (grey bounds) are calculated across all water parcels within which phytoplankton growth occurs. The green and blue lines are examples of the autocorrelations of two different water parcels; the nitrate concentration and trajectories of these two water parcels are shown in plots: b, c, and d. (b) Time series of nitrate concentrations starting when nitrate uptake occurs (t = 0), followed by nitrate concentrations along the backward water parcel trajectory (i.e., during days before phytoplankton growth); the black asterisk indicates the nitrate memory time. (c and d) Water parcel trajectories colored by nitrate concentration, the black asterisk indicates the geographical location of the nitrate source (i.e., GAB-SAFn in Figure 3c and GAB in Figure 4d), dates encompassing the water parcel trajectories are shown.

2.5. Phytoplankton Growth

Phytoplankton concentrations are transformed to chlorophyll-a concentrations considering that 1 mmol of N is equivalent to 1.59 mg of chlorophyll-a (Matear et al., 2013). Instances of an increase in chlorophyll-a concentration and a decline in nitrate concentration along water parcel trajectories are identified as instances of phytoplankton growth.

The geographical location, date, nitrate, and chlorophyll-a concentrations as well as the daily change in chlorophyll-a concentration for each instance of phytoplankton growth are recorded and used to examine their spatial (vertical and horizontal) distribution, intensity, and variation in time.

Specifically, we construct horizontal spatial distribution maps of instances of phytoplankton growth (including all depths where phytoplankton growth can occur, i.e., 1–180 m), and their magnitude. Average primary productivity is controlled by regional and seasonal trends rather than by high frequency variability (Bissett et al., 1994); therefore, we focus our attention on climatologies of mean chlorophyll-a concentration and daily change in chlorophyll-a concentration (i.e., phytoplankton growth) throughout the water column; additionally, spectral analysis is applied to 12 years (1993–2005) of chlorophyll-a concentration and daily change of chlorophyll-a concentration to ascertain dominant periodicities of phytoplankton growth.

3. Results

3.1. Nitrate Local Sources

Nitrate concentrations along water parcel backward trajectories (i.e., before nitrate is taken up by phytoplankton to grow, Figure 3) can increase due to local decomposition and consequent organic matter

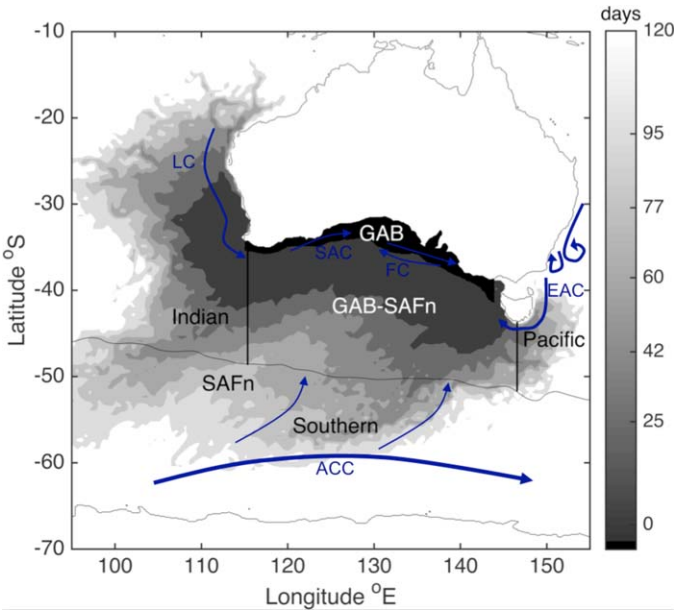

Figure 4. Map of the minimum time it takes water parcels to reach the GAB depending their location; the color labels correspond to the map contours shown. Arrows represent the mean currents in the region: Leeuwin Current (LC), South Australia Current (SAC), subsurface Flinders Current (FC), Antarctic Circumpolar Current (ACC), and East Australian Current (EAC).

remineralization, or decrease due to consumption. From all the growth instances, the averaged nitrate memory time is 59 ± 17 days (Figure 3a). Backward trajectories of water parcels show that 59 days before nitrate uptake and phytoplankton growth, water parcels are often inside the GAB or in the GAB-SAFn (Figures 3 and 4); in fact, 23% and 75% of phytoplankton growth instances are sustained by nitrate sources from the GAB and SAFn, respectively. Thus, the vast majority of the nitrate used by phytoplankton to grow in the GAB is local and shows the importance of locally recycled nitrate to sustaining phytoplankton growth.

Our results do show that in some parts of the GAB, the nitrate is occasionally sourced from outside of the GAB and SAFn. Although infrequently, nitrate sourced from adjacent oceans is occasionally (2%) used by phytoplankton in the GAB without first being recycled in the region. In the eastern GAB, phytoplankton growth is very sporadically fueled by nitrate sourced from the Pacific or Southern Oceans, while in the western GAB, phytoplankton growth is fueled more regularly from nitrate sourced from the Indian Ocean. As shown by the map of the minimum time required for water parcels to reach the GAB depending on their location, water parcels from the Pacific, Southern, and Indian Oceans can reach the GAB in 59 days (Figure 4).

The Pacific and Southern Oceans act as an occasional nitrate source (i.e., $<$0.1%) in winter-spring and these instances are high in nitrate concentrations and associated with large phytoplankton growth events. Conversely, contributions from the Indian Ocean occur year-round but are not commonly associated with either high nitrate concentrations or high phytoplankton growth (Figure 5).

Furthermore, at the nitrate memory time, the water parcels are typically (79%) above 100 m of depth, and occasionally (21%) below 100 m and above 430 m. Deep-water (100–430 m) parcels are associated with higher nitrate concentrations than those above 100 m. The difference is largest during the Australian autumn (centered in March–April, Figure 6); in June–July phytoplankton growth is higher below 100 m.

3.2. Nitrate Supply

To provide a perspective on how nitrate enters the GAB and SAFn regions, we compute the monthly climatology of the nitrate transport into these two regions through their boundaries (Figure 7).

Nitrate input to the GAB occurs mostly through the southern but also through the western and eastern boundaries; specifically, it flows through most of the water column in the southern boundary (0–400 and 1,000–2,000), in the top 300 m through the western boundary, and between 400 and 1,000 m in the eastern boundary (Figure 7a1). Not surprisingly, nitrate flux into the GAB is greater from below 100 m than above 100 m (Figure 7a2) with most of the nitrate entering between 100 and 300 m and between 1,000 and 2,000 m.

The strong seasonality to the transport supports our Lagrangian analysis that recycled nitrate generally sustains phytoplankton growth instances. Only in January and from June to December is there a net transport of nitrate into the GAB (Figure 7a2), over these time periods phytoplankton growth instances are, therefore, also linked to nitrate sourced outside the GAB or GAB-SAFn; specifically from the Southern or Pacific Oceans (Figure 5). Conversely, from February to May, there is no net transport of nitrate into the GAB and phytoplankton growth must be fueled by nitrate that is being recycled within the GAB.

For the GAB-SAFn region, nitrate is supplied through the western boundary between 0 and 3,000 m, and through the southern boundary in the top 20 m (Figure 7b). The GAB-SAFn region, nitrate flux displays prominent seasonal variability with a maximum flux into the region in the August–September period through the entire water column (Figure 7b).

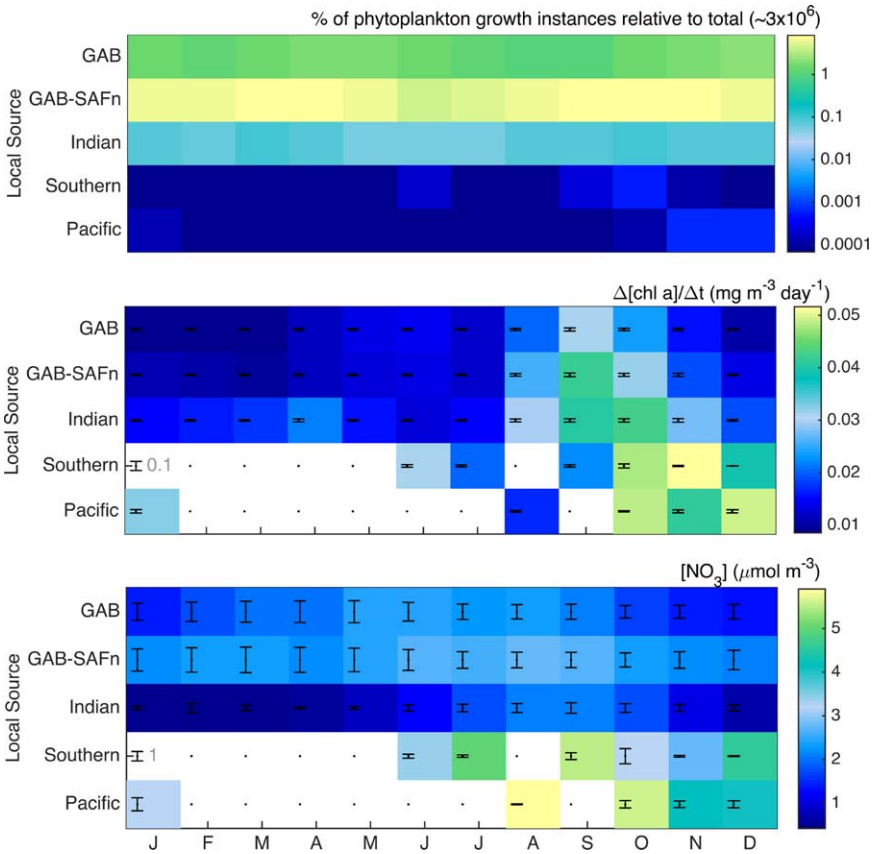

Figure 5. (a) Monthly climatologies of the % of instances of phytoplankton growth sorted by nitrate sources; the color-scale logarithmic. Mean (colorbar) and standard error (bars) monthly climatologies of (b) daily changes in chlorophyll-a concentration, and (c) nitrate concentration, across instances of phytoplankton growth from 1993 to 2005 sorted by local nitrate source (i.e., Pacific, Southern, Indian ocean, SAFn-GAB, GAB).

3.3. Phytoplankton Growth

Over 12 years (1992–2005) we identified $\sim 3 \times 10^6$ instances of phytoplankton growth; they occur throughout the GAB but congregate between the 70 and 2,000 m isobaths. Mean chlorophyll-a concentrations across all instances of phytoplankton growth are similar throughout the GAB ($\sim$0.3–0.4 mg m^{-3}, Figure 8), with the maximum values close to the coastline west of the GAB's head, and south of Eyre Peninsula ($\sim$137°E longitude). The spatial distribution of the largest phytoplankton growth (daily change in chlorophyll-a concentration) shows more structure and appears related to the GAB's topography (Figure 8b). The maximum increase of 0.35 mg m^{-3} d^{-1} occurs between 500 and 2,000 m isobaths where the mean upward displacement of water parcels associated with phytoplankton growth is nearly (20 m d^{-1}, Figure 8c). As one moves closer to the coast the mean upward displacement is much smaller (0–5 m d^{-1}) and maximum increase in daily chlorophyll is much smaller (Figures 8c and 8d).

The depth at which chlorophyll-a concentration and phytoplankton growth are largest varies with seasons. Half of the year, during summer months (December–March) and early winter (June–July) chlorophyll-a peaks close to the surface (<6.5 m); the rest of the year there is a subsurface (i.e., below 10.5 m) maximum, being deepest (26 m) in autumn (May) and between 10.5 and 18.5 m deep in April, August–November (Figure 8). Maximum phytoplankton growth occurs near the surface (2.5 m) in late summer (February–March) and at the end of winter (August–September); otherwise, maximum phytoplankton growth occurs below the surface at intermediate depths (8.5–10.5 m) from October to January, and at depth during autumn-winter; particularly, in April the maximum phytoplankton growth occurs at 66 m and continues deepening to a depth of 148 m by July. The deepening of the maximum phytoplankton growth follows that of the mixed layer depth within the GAB (Figure 9).

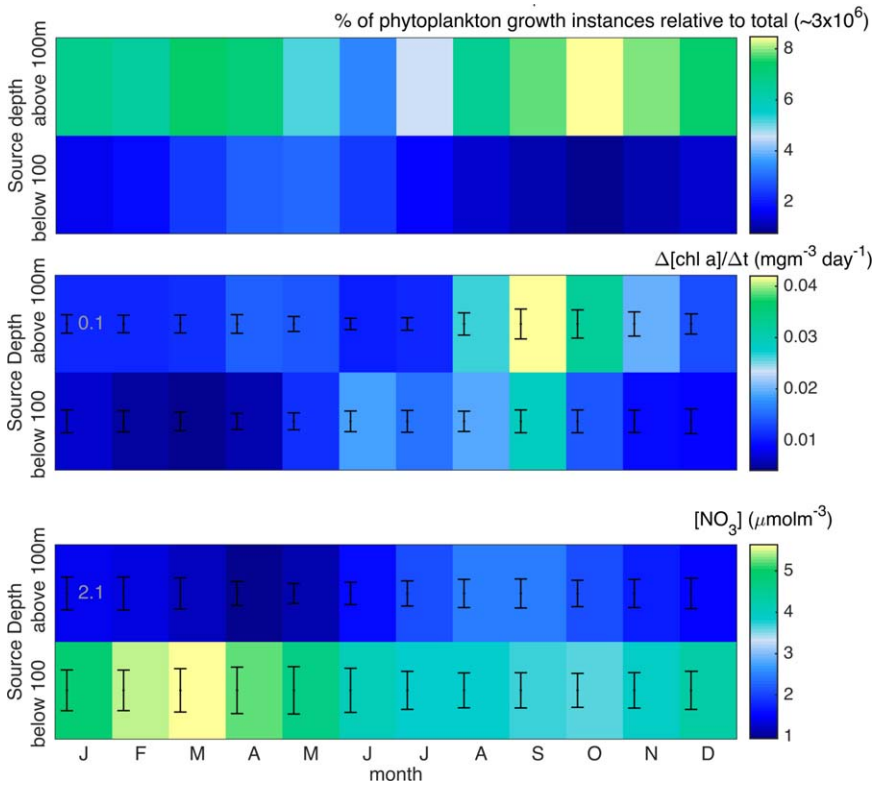

Figure 6. (a) Monthly climatologies of the % of instances of phytoplankton growth sorted by local nitrate source depth. Mean (colorbar) and standard error (bars) monthly climatologies of (b) daily changes in chlorophyll-a concentration, and (c) nitrate concentration, across instances of phytoplankton growth from 1993 to 2005 sorted by local nitrate source depth (i.e., $<$100 and $>$100 m).

In the GAB, both chlorophyll-a concentration, and phytoplankton growth have a prominent annual periodicity at most depths with a maximum in September (Figure 10). However, between 60 and 100 m, the annual periodicity is not significant and instead, a semiannual periodicity, driven by peaks in phytoplankton growth in early spring (September), and autumn to early winter occur (Figure 10).

4. Discussion

We have diagnosed the sources of nitrate for phytoplankton growth in the GAB using 12 years outputs of a coupled hydrodynamic-biogeochemical model. Our study exemplifies advantages of an Eulerian-Lagrangian approach to examine biogeochemical processes in the ocean. The Lagrangian component of our study permits identifying increases in phytoplankton concentration caused by phytoplankton growth rather than by biomass advection. Further, determining the water parcel back-trajectories preceding phytoplankton growth provides insight into mechanisms facilitating phytoplankton growth (e.g., topographical uplift). Finally, we define the concept of memory time; this concept establishes a time limit to track water parcels, backward in time, before determining the origin of nitrate. Because water parcel trajectories could be tracked indefinitely, without the nitrate memory time definition, the concept of origin in Lagrangian analysis would be ambiguous. The nitrate memory time (59 days for the GAB in our model) is then used to identify the sources of nitrate fueling phytoplankton growth. We find that the overwhelming majority of phytoplankton growth in our model (98%) is fueled by nitrate recycled within the GAB and the adjacent GAB-SAFn region rather than directly supplied from oceans afar.

4.1. Nitrate Sources and Supply into the GAB

The geography and prevailing circulation in the region influence the local sources of nitrate. The Indian Ocean acts as a local source of nitrate for phytoplankton growth more often ($\sim$1%) than other Oceans ($<$0.1%) surrounding the GAB through the intrusion of the poleward flowing Leeuwin Current into south

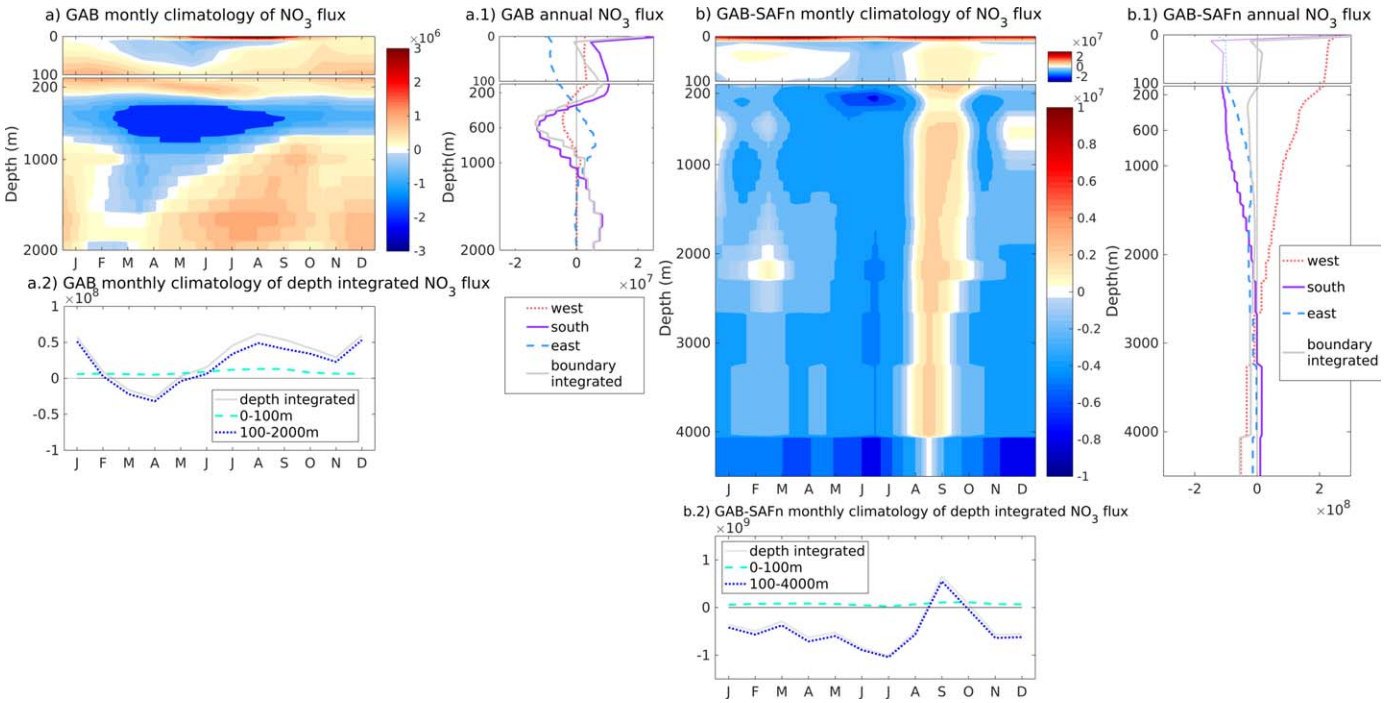

Figure 7. Climatologies of nitrate flux (μmol N s^{-1}, colorbar) in (+) and out (−) of the (a) GAB and (b) GAB-SAFn boxes integrated across all boundaries. Annual nitrate fluxes through the GAB (a1) and GAB-SAFn boundaries (east, west, and south). Depth integrated monthly climatologies of nitrate flux for the GAB (a2) and GAB-SAFn (b2).

Australia, and the presence of the eastward flowing South-Australia surface current (Coleman et al., 2013; Hanson et al., 2005; Herzfeld & Tomczak, 1997; Ridgway & Condie, 2004; Yit Sen Bull & van Sebille, 2016, Figure 4). However, nitrate concentrations in the Indian Ocean and the Leeuwin Current are low (Dietze et al., 2009); hence, this source of nitrate can only induce small phytoplankton growth instances (Figure 5).

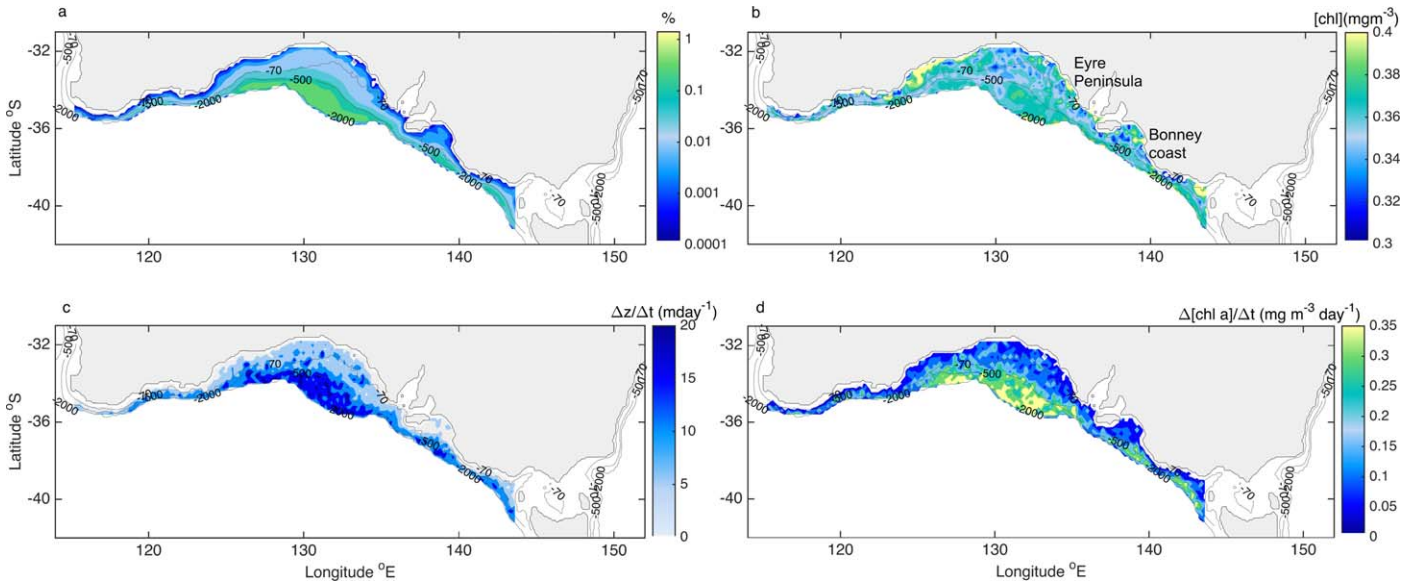

Figure 8. GAB horizontal spatial distribution maps of (a) instances of phytoplankton growth from 1992 to 2005 in percentage relative to the total, (b) mean chlorophyll-a concentration across phytoplankton growth instances, (c) mean change in depth of water parcels associated with upwelling and phytoplankton growth instances, and (d) maximum change in chlorophyll-a concentration across phytoplankton growth instances. Instances of phytoplankton growth are binned into 0.2° × 0.2° cells.

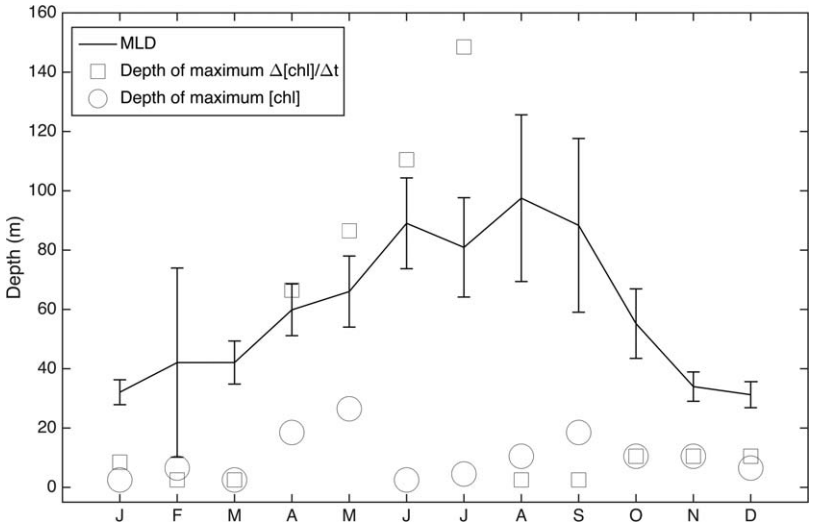

Figure 9. Climatology of depths where maximum phytoplankton growth (squares) and maximum chlorophyll-a concentration (circles) occur. Error bars show the mean and standard deviation of the mixed layer depth within the GAB from de Boyer Montégut et al. (2004).

In contrast, the Southern Ocean has high nitrate concentrations, and the phytoplankton growth that it fuels within the GAB is large in magnitude. However, this rarely occurs except for a few times between winter and spring when seasonal wind speeds between Australia and Antarctica are stronger (e.g., Luis & Pandey, 2004), potentially intensifying the Ekman flow from the Southern Ocean into the GAB and the delivery of nitrate from the Southern Ocean into the GAB. These results suggest that a positive Southern Annual Mode (SAM), which implies a southward shift and intensification of the southern hemisphere westerlies (e.g., Thompson & Wallace, 2000), could facilitate the supply of more nutrient rich Subantarctic Mode Water (SAMW) to the GAB and enhance primary productivity. Ayers and Strutton (2013) have observed this mechanism in the Pacific sector of the Southern Ocean.

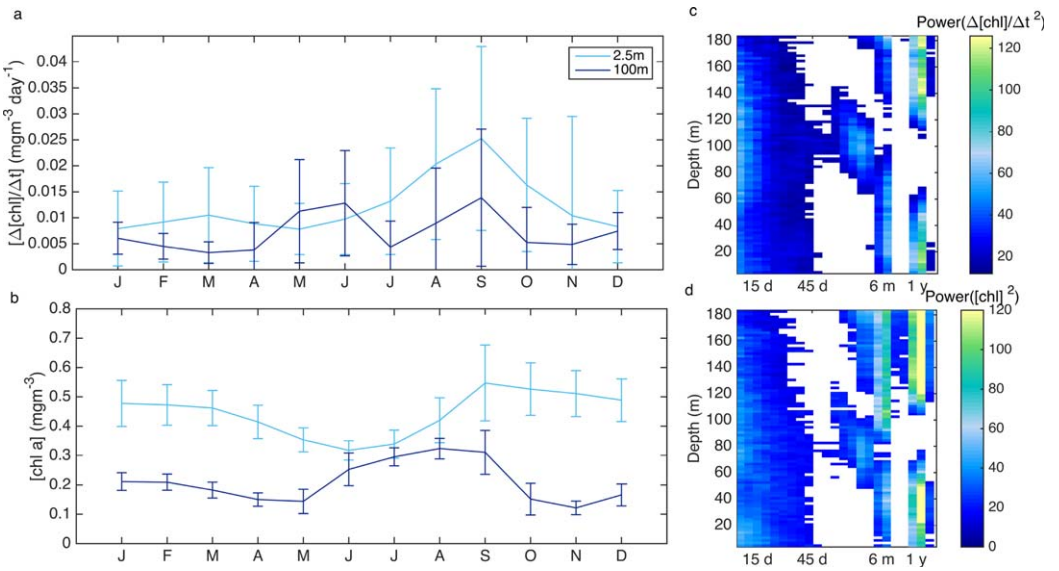

Figure 10. Within the GAB the mean and standard error climatologies of (a) daily change in chlorophyll-a concentration and (b) chlorophyll-a concentration, across instances of phytoplankton growth from 1993 to 2005 sorted by depth (i.e., 2.5 and 100 m). Within the GAB the power spectrum (colorbar) of (c) daily change in chlorophyll-a concentration and (d) chlorophyll concentration at each depth. Only significant periodicities are shown. The global power spectrum is calculated using code from Torrence and Compo (1998) and Liu et al. (2007) bias correction.

Insight into the nitrate supply to the GAB by different oceans in our model is gained from our Eulerian-Lagrangian approach. Together, particle trajectories and nitrate fluxes, support the conclusion that most of the water entering the GAB comes from either the Southern or Indian Oceans rather than the Pacific. The main pathways of Southern and Indian Ocean waters into the GAB are through the west and south boundaries of the GAB and GAB-SAFn (Figure 5); these are also the boundaries with the largest nitrate flux into the GAB and GAB-SAFn (Figure 7). Differently, water from the Pacific Ocean enters the GAB through its eastern boundary below 400 m where nitrate fluxes are lower (Figure 7). Because nitrate concentrations are higher in Southern than Indian Ocean waters (Condie & Dunn, 2006) our results imply that most of the nitrate transported into the GAB is originally supplied by the Southern Ocean.

4.2. Nitrate Input Over Depth and Supply Mechanisms for Phytoplankton Growth

Most of the nitrate enters the GAB at depth but local nitrate sources that account for 79% of the phytoplankton growth are in the top 100 m (Figures 7a2 and 5). In addition, phytoplankton growth can only occur in the presence of light; therefore, there must be mechanisms inside the GAB delivering nitrate from deep waters into the euphotic zone. Our results show that topographical uplift as well as stratification erosion facilitate the supply of nutrients into a depth shallow enough for phytoplankton growth to occur.

We find maximum phytoplankton growth along the shelf break coinciding with a region where upward water displacement is largest (Figures 8c and 8d). These results suggest that in addition to localized wind-induced upwelling (e.g., Kämpf et al., 2004), topographical upwelling may lead to considerable phytoplankton growth within the GAB. Supporting this hypothesis, water-cooling events in the absence of upwelling favorable winds have been reported in the eastern GAB (e.g., Griffin et al., 1997; Kämpf, 2010); similarly, water upwelled below the mixed layer depth but within the euphotic zone induces deep chlorophyll maxima (van Ruth et al., 2010). Moreover, studies of the circulation in the region show the interaction with the bottom of the westward flowing subsurface Flinders Current (centered along the shelf break) is upwelling favorable (Middleton & Bye, 2007; Richardson et al., 2009; van Ruth, 2009); Similarly, Herzfeld and Tomczak (1997) found that flow strengthening and consequent bottom stress intensification west of Eyre Peninsula (∼137°E longitude) induces bottom boundary layer upwelling, which can exceed upwelling driven by the winds (Middleton & Platov, 2003). Importantly, a strengthening of the Flinders Current has occurred over the last several decades (Feng et al., 2016) and such an intensification could increase primary productivity in the GAB through enhanced current driven upwelling and nitrate supply into the euphotic zone.

Furthermore, below 100 m, phytoplankton growth is largest from June to September when enhanced winds and surface heat loss reduce stratification and the mixed layer deepens (Condie & Dunn, 2006). Conversely, episodes associated with shallow water (above 100 m) occur year-round and peak in spring (Figure 6) when stratification starts to re-establish. Therefore, a second mechanism enabling nitrate entrainment above the nutricline and leading to phytoplankton growth within the GAB is weak stratification.

4.3. Phytoplankton Growth Climatology

Focusing on patterns of phytoplankton growth that is consistent throughout the GAB, climatologies of chlorophyll-a and its daily changes are calculated at different depths across all instances of phytoplankton growth within the region. We found evidence of a canonical spring-autumn phytoplankton growth with both chlorophyll-a concentrations and phytoplankton growth peaking in spring throughout the water column (Figure 10); such periodicities have persisted over 12 years (1993–2005). The occurrence of localized coastal summer blooms has a limited impact on the seasonal signal, and it is only evident at the surface where maximum phytoplankton growth occurs in spring followed by summer. Conversely, at depth, phytoplankton growth is greatest in spring and autumn. The spring-autumn pattern usually emerges as a result of stratification breakdown in autumn, which makes nutrients accumulated below the summer pycnocline available for uptake, and seasonal increase in solar radiation during spring (e.g., Cloern, 1996; Cushing, 1959; Longhurst, 1995). Indeed, the mixed layer deepens in autumn-winter reaching ∼60–100 m in the middle of the GAB (Condie & Dunn, 2006; de Boyer Montégut et al., 2004).

Recently, Kämpf and Kavi (2017) examined satellite-derived monthly chlorophyll-a concentrations and found moderate phytoplankton blooms widespread in southern Australian shelves during autumn and early winter. In agreement, our results support the occurrence of considerable phytoplankton growth within the GAB during autumn; furthermore, they show that autumn phytoplankton growth peaks at depth and is

associated with a semiannual periodicity. We show that both chlorophyll-a and phytoplankton growth have a subsurface maximum for 6 and 8 months of the year, respectively (Figure 9). The deepening of maximum phytoplankton growth follows the mixed layer depth (Figure 9) suggesting that mixing and loss of stratification supplies deep nutrient rich water into the euphotic zone inducing large phytoplankton growth at depth. The subsurface maximums of chlorophyll-a and phytoplankton growth within the GAB evidenced in this study highlight the importance of complementing satellite-derived chlorophyll-a with model outputs or observations at depth when examining ocean productivity.

Acknowledgments

OFAM-WOMBAT is produced by the Commonwealth Scientific and Industrial Research Organization (CSIRO) and the data used are available at http://www.cmar.csiro.au/thredds/catalog/OFAM3_BGC_SPINUP_01/. Daily chlorophyll-a concentrations can be ordered at: http://hermes.acri.fr. Mixed layer depth climatologies are available at: http://www.ifremer.fr/cerweb/deboyer/mld/home.php. Wavelet software was provided by C. Torrence and G. Compo, and it is available at URL: http://atoc.colorado.edu/research/wavelets. Matlab code for the bias correction by Liu et al. (2007) is available in ocg6.marine.usf.edu/~liu/wavelet.html. This work was funded by the ARC via grant DE130101336. P.C.H. was partially supported by an Australian Research council linkage grant LP150100064. We thank colleagues from the Climate Change Research Centre, UNSW for their feedback.

References

Ayers, J. M., & Strutton, P. G. (2013). Nutrient variability in Subantarctic Mode Waters forced by the southern annular mode and ENSO. *Geophysical Research Letters*, *40*, 3419–3423. https://doi.org/10.1002/grl.50638

Behrenfeld, M. J., & Falkowski, P. G. (1997). Photosynthetic rates derived from satellite-based chlorophyll concentration. *Limnology and Oceanography*, *42*(1), 1–20.

Bissett, W. P., Meyers, M. B., Walsh, J. J., & Muller-Karger, F. E. (1994). The effects of temporal variability of mixed layer depth on primary productivity around Bermuda. *Journal of Geophysical Research: Oceans*, *99*, 7539–7553. https://doi.org/10.1029/93JC03154

Boyd, P. W., Strzepek, R., Fu, F., & Hutchins, D. A. (2010). Environmental control of open-ocean phytoplankton groups: Now and in the future. *Limnology and Oceanography: Methods*, *55*(3), 1353–1376.

Chenillat, F., Blanke, B., Grima, N., Franks, P. J., Capet, X., & Rivière, P. (2015). Quantifying tracer dynamics in moving fluids: A combined Eulerian-Lagrangian approach. *Frontiers of Environmental Science*, *3*, 43.

Cloern, J. E. (1996). Phytoplankton bloom dynamics in coastal ecosystems: A review with some general lessons from sustained investigation of San Francisco Bay, California. *Reviews of Geophysics*, *34*, 127.

Coleman, M. A., Feng, M., Roughan, M., Cetina-Heredia, P., & Connell, S. D. (2013). Temperate shelf water dispersal by Australian boundary currents: Implications for population connectivity. *Limnology and Oceanography: Methods*, *3*, 295–309.

Condie, S. A., & Dunn, J. R. (2006). Seasonal characteristics of the surface mixed layer in the Australasian region: Implications for primary production regimes and biogeography. *Marine and Freshwater Research*, *57*, 569–590.

Cushing, D. H. (1959). The seasonal variation in oceanic production as a problem in population dynamics. *Journal Du Conseil*, *24*, 455–464.

de Boyer Montégut, C., Madec, G., Fischer, A. S., Lazar, A., & Iudicone, D. (2004). Mixed layer depth over the global ocean: An examination of profile data and a profile-based climatology. *Journal of Geophysical Research: Oceans*, *109*, C12003. https://doi.org/10.1029/2004JC002378

Dietze, H., Matear, R. J., & Moore, T. (2009). Nutrient supply to anticyclonic meso-scale eddies off western Australia estimated with artificial tracers released in a circulation model. *Deep-Sea Research Part I*, *56*(9), 1440–1448. https://doi.org/10.1016/j.dsr.2009.04.012

Dimmlich, W. F., Breed, W. G., Geddes, M., & Ward, T. M. (2004). Relative importance of gulf and shelf waters for spawning and recruitment of Australian anchovy, *Engraulis australis*, in South Australia. *Fisheries Oceanography*, *13*(5), 31–323.

D'Ortenzio, F., Lavigne, H., Besson, F., Claustre, H., Coppola, L., Garcia, N.,. . . Testor, P. (2014). Observing mixed layer depth, nitrate and chlorophyll concentrations in the northwestern Mediterranean: A combined satellite and NO_3 profiling floats experiment. *Geophysical Research Letters*, *41*, 6443–6451. https://doi.org/10.1002/2014GL061020

Falkowski, P. G., & Kolber, Z. (1995). Variations in chlorophyll fluorescence yields in phytoplankton in the world oceans. *Australian Journal of Plant Physiology*, *22*, 341–355.

Feng, M., Zhang, X., Oke, P., Monselesan, D., Chamberlain, M. A., Matear, R. J., & Schiller, A. (2016). Invigorating ocean boundary current systems around Australia during 1979–2014: As simulated in a near-global eddy-resolving ocean model. *Journal of Geophysical Research: Oceans*, *121*, 3395–3408. https://doi.org/10.1002/2016JC011842.

Gill, P. C., Morrice, M. G., Page, B., Pirzl, R., Levings, A. H., & Coyne, M. (2011). Blue whale habitat selection and within-season distribution in a regional upwelling system off southern Australia. *Marine Ecology Progress Series*, *421*, 243–263. https://doi.org/10.3354/meps08914

Graham, R. M., De Boer, A. M., van Sebille, E., Kohfeld, K. E., & Schlosser, C. (2015). Inferring source regions and supply mechanisms of iron in the Southern Ocean from satellite chlorophyll data. *Deep-Sea Research Part I*, *104*, 9–25.

Griffin, D. A., Thompson, P. A., Bax, N. J., & Hallegraeff, G. M. (1997). The 1995 mass mortality of pilchards: No role found for physical or biological oceanographic factors in Australia. *Australian Journal of Marine and Freshwater Research*, *48*, 27–58.

Hanson, C. E., Pattiaratchi, C. B., & Waite, A. M. (2005). Seasonal production regimes off south-western Australia: Influence of the Capes and Leeuwin Currents on phytoplankton dynamics. *Marine and Freshwater Research*, *56*, 1011–1026. https://doi.org/10.1071/MF04288

Herzfeld, M., & Tomczak, M. (1997). Numerical modelling of sea surface temperature and circulation in the Great Australian Bight. *Progress in Oceanography*, *39*, 29–78.

Jönsson, B. F., & Salisbury, J. E. (2016). Episodicity in phytoplankton dynamics in a coastal region. *Geophysical Research Letters*, *43*, 5821–5828. https://doi.org/10.1002/2016GL068683

Jönsson, B. F., Salisbury, J. E., & Mahadevan, A. (2011). Large variability in continental shelf production of phytoplankton carbon revealed by satellite. *Biogeosciences*, *8*, 1213–1223.

Kämpf, J. (2010). On preconditioning of coastal upwelling in the eastern Great Australian Bight. *Journal of Geophysical Research: Oceans*, *115*, C12071. https://doi.org/10.1029/2010JC006294

Kämpf, J., Doubell, M., Griffin, D., Matthews, R. L., & Ward, T. M. (2004). Evidence of a large seasonal coastal upwelling system along the Southern Shelf of Australia. *Geophysical Research Letters*, *31*, L09310. https://doi.org/10.1029/2003GLO19221

Kämpf, J., & Kavi, A. (2017). On the "hidden" phytoplankton blooms on Australia's southern shelves. *Geophysical Research Letters*, *44*, 1466–1473. https://doi.org/10.1002/2016GLO72096

Kidston, M., Matear, R. J., & Baird, M. E. (2011). Parameter optimization of a marine ecosystem model at two contrasting stations in the Sub-Antarctic Zone. *Deep-Sea Research Part II*, *58*, 2301–2315.

Laiolo, L., McInnes, A. S., Matear, R. J., & Doblin, M. (2016). Key drivers of seasonal plankton dynamics in cyclonic and anticyclonic eddies off East Australia. *Frontiers in Marine Science*, *3*, 155. https://doi.org/10.3389/fmars.2016.00155

Lavigne, H., D'ortenzio, F., Claustre, H., & Poteau, A. (2012). Towards a merged satellite in situ fluorescence ocean chlorophyll product. *Biogeosciences*, *9*, 2111–2125. https://doi.org/10.5194/bg-9-2111-2012

Lewis, R. K. (1981). Seasonal upwelling along the southeastern coastline of South Australia, *Australian Journal of Marine and Freshwater Research*, *32*, 843–854.

Liu, Y., San Liang, X., & Weisberg, R. (2007). Rectification of the bias in the wavelet power spectrum. *Journal of Atmospheric and Oceanic Technology*, *24*, 2093–2102. https://doi.org/10.1175/2007JTECHO511.1

Longhurst, A. (1995). Seasonal cycles of pelagic production and consumption. *Progress in Oceanography*, *36*, 77–167.

Luis, A. J., & Pandey, P. C. (2004). Seasonal variability of QSCAT-derived wind stress over the Southern Ocean. *Geophysical Research Letters*, *31*, L13304. https://doi.org/10.1029/2003GL019355

Matear, R. J., Chamberlain, M. A., Sun, C., & Feng, M. (2013). Climate change projection of the Tasman Sea from an Eddy-resolving Ocean Model. *Journal of Geophysical Research: Oceans*, *118*, 2961–2976. https://doi.org/10.1002/jgrc.20202

Matear, R. J., Chamberlain, M. A., Sun, C., & Feng, M. (2015). Climate change projection for the western tropical Pacific Ocean using a high-resolution ocean model: Implications for tuna fisheries. *Deep-Sea Research Part II*, *113*, 22–46. https://doi.org/10.1016/j.dsr2.2014.07.003

McClatchie, S., Middleton, J. F., & Ward, T. M. (2006). Water mass analysis and alongshore variation in upwelling intensity in the eastern Great Australian Bight. *Journal of Geophysical Research: Oceans*, *111*, C08007. https://doi.org/10.1029/2004JC002699

Middleton, J. F., & Bye, J. A. T. (2007). A review of the shelf-slope circulation along Australia's southern shelves: Cape Leeuwin to Portland. *Progress in Oceanography*, *75*, 1–41.

Middleton, J. F., & Platov, G. (2003). The mean summertime circulation along Australia's Southern Shelves: A numerical study. *Journal of Physical Oceanography*, *33*, 2270–2287.

Moore, C. M., Mills, M. M., Arrigo, K. R., Berman-Frank, I., Bopp, L., Boyd, P. W.,. . . Ulloa, O. (2013). Processes and patterns of oceanic nutrient limitation. *Nature Geoscience*, *6*, 701–710.

Oke, P. R., Griffin, D. A., Schiller, A., Matear, R. J., Fiedler, R., Mansbridge, J.,. . . Ridgway, K. R. (2013). Evaluation of a near-global eddy-resolving ocean model. *Geoscientific Model Development*, *6*, 591–615.

Paris, C. B., Helgers, J., van Sebille, E., & Srinivasan, A. (2013). The connectivity modelling system: A probabilistic tool for the multi-scale tracking of biotic and abiotic variability in the ocean. *Environmental Modelling & Software*, *42*, 47–54. https://doi.org/10.1016/j.envsoft.2012.12.006

Petrusevics, P., Bye, J. A. T., Fahlbusch, V., Hammat, J., Tippins, D. R., & van Wijk, E. (2009). High salinity winter outflow from a mega inverse estuary—The Great Australian Bight. *Continental Shelf Research*, *29*, 371–380.

Qin, X., Menviel, L., Sen Gupta, A., & van Sebille, E. (2016). Iron sources and pathways into the Equatorial Pacific. *Geophysical Research Letters*, *43*, 9843–9851. https://doi.org/10.1002/2016GL070501

Qin, X., Sen Gupta, A., & van Sebille, E. (2015). Variability in the origins and pathways of Pacific Equatorial Undercurrent water. *Journal of Geophysical Research: Oceans*, *120*, 3113–3128. https://doi.org/10.1002/2014JC010549

Richardson, L. E., Kyser, T. K., James, N. P., & Bone, Y. (2009). Analysis of hydrographic and stable isotope data to determine water masses, circulation, and mixing in the Easter Great Australian Bight. *Journal of Geophysical Research: Oceans*, *114*, C10016. https://doi.org/10.1029/2009JC005407

Ridgway, K. R., & Condie, S. A. (2004). The 5500-km long boundary flow off western and southern Australia. *Journal of Geophysical Research: Oceans*, *109*, C04017. https://doi.org/10.1029/2003JC001921

Ridgway, K. R., & Dunn, J. R. (2003). Mesoscale structure of the mean East Australian Current System and its relationship with topography. *Progress in Oceanography*, *56*, 189–222.

Sallée, J. B., Morrow, R., & Speer, K. (2008). Response of the Antarctic Circumpolar Current to atmospheric variability. *Journal of Climate*, *21*, 3020–3039.

Sun, C., Feng, M., Matear, R. J., Chamberlain, M. A., Craig, P., Ridgway, K. R., & Schiller, A. (2012). Marine downscaling of a future climate scenario for Australian boundary currents. *Journal of Climate*, *25*, 2947–2962.

Talley, L. D., Pickard, G. L., Emery, W. J., & Swift, J. H. (2011). Data analysis concepts and observational methods. In *Descriptive physical oceanography: An introduction* (6th ed., pp. 155–160). London, UK: Elsevier.

Thompson, D. W. J., & Wallace, J. M. (2000). Annular modes in the extratropical circulation. Part I: Month-to-month variability. *Journal of Climate*, *13*, 1000–1016.

Torrence, C., & Compo, G. P. (1998). A practical guide to wavelet analysis. *Bulletin of the American Meteorological Society*, *79*(1), 61–78.

van Ruth, P. D. (2009). *Spatial and temporal variation in primary and secondary productivity in the eastern Great Australian Bight* (PhD thesis). Adelaide, Australia: School of Earth and Environmental Sciences, The University of Adelaide.

van Ruth, P. D., Ganf, G. G., & Ward, T. M. (2010). Hot-spots of primary productivity: An alternative interpretation to conventional upwelling models. *Estuarine, Coastal and Shelf Science*, *90*, 142–158.

Wadley, M. R., Jickells, T. D., & Heywood, K. J. (2014). The role of iron sources and transport for Southern Ocean productivity. *Deep-Sea Research Part I*, *87*, 82–94.

Ward, T. M., McLeay, L. J., Dimmlich, W., Rogers, A., McClatchie, S., Matthews, R. L., Kämpf, J., & Van Ruth, P. D. (2006). Pelagic ecology of a northern boundary current system: Effects of upwelling on the production and distribution of sardine (*Sardinops sagax*), anchovy (*Engraulis australis*) and southern bluefin tuna (*Thunnus maccoyii*) in the Great Australian Bight. *Fisheries Oceanography*, *15*, 191–207.

Williams, R. G., & Follows, M. J. (2003). Physical transport of nutrients and the maintenance of biological production. In M. J. R. Fasham (Ed.), *Ocean biogeochemistry* (chap. 2, pp. 19–51). New York, NY: Springer-Verlag.

Xing, X.-G., Zhao, D.-Z., Liu, Y.-G., Yang, J.-H., Xiu, P., & Wang, L. (2007). An overview of remote sensing chlorophyll fluorescence. *Ocean Science Journal*, *42*(1), 49–59.

Yit Sen Bull, C., & van Sebille, E. (2016). Sources, fate, and pathways of Leeuwin Current water in the Indian Ocean and Great Australian Bight: A Lagrangian study in an eddy-resolving ocean model. *Journal of Geophysical Research: Oceans*, *121*, 1626–1639. https://doi.org/10.1002/2015JC011486

Zhang, X., Oke, P. R., Feng, M., Chamberlain, M. A., Church, J. A., Monselesan, D.,. . . Fiedler, R. (2016). A near-global eddy-resolving OGCM for climate studies. *Geoscientific Model Development Discussions*, 1–52. https://doi.org/10.5194/gmd-2016-17